Diamond & Related Materials 18 (2009) 220–223

Contents lists available at ScienceDirect

Diamond & Related Materials

journal homepage: www.elsevier.com/locate/diamond

Magnetic and EPR studies of edge-localized spin paramagnetism in multi-shell nanographites derived from nanodiamonds

V.Yu. Osipov [a,b,*], A.I. Shames [c], T. Enoki [d], K. Takai [d], M. Endo [e], T. Hayashi [e], Y. Kaburagi [f], A.Ya. Vul' [a]

[a] Ioffe Physico-Technical Institute, Polytechnicheskaya 26, St. Petersburg, 194021, Russia
[b] Faculty of Electronics, St. Petersburg Electrotechnical University "LETI", Prof. Popov str.5, St. Petersburg, 197376, Russia
[c] Department of Physics, Ben-Gurion University of the Negev, Be'er-Sheva 84105, Israel
[d] Department of Chemistry, Tokyo Institute of Technology, 2-12-1, Ookayama, Meguro-ku, Tokyo 152-8551, Japan
[e] Faculty of Engineering, Shinshu University, Nagano-shi 380-8553, Japan
[f] Department of Energy Science and Engineering, Musashi Institute of Technology, Setagaya-ku, Tokyo 158-8557, Japan

ARTICLE INFO

Available online 11 September 2008

Keywords:
Graphite nanoparticles
Edge electronic states
Magnetic susceptibility
Electron paramagnetic resonance

ABSTRACT

Prolonged (up to 2 h) heat treatment at 1600 °C of nanodiamond particles (5 nm) leads to their conversion to the mixture of quasi-spherical carbon onions and multi-shell polyhedral nanographites. Structural and magnetic properties of two (A and B) series of nanographite samples obtained at various annealing intervals were studied. XRD data show that both multi-shell nanographite samples have practically the same crystalline structures. HRTEM evidences that the most of particles obtained by short time (7 min) annealing have a spherical like shape whereas the long time (~2 h) annealing leads to the majority of particles having a polyhedral shape with a hollow inside. Electronic and magnetic properties of these nanocarbons were investigated by magnetic susceptibility and EPR. Annealing results in entire transformation of the EPR signal of nanodiamond to new EPR signals of various line shapes and widths. These signals are extremely sensitive to ambient oxygen. Concentrations for all EPR active spins vary from ~1×10^{19} spins/g (7 min) to ~2×10^{19} spins/g (2 h). Temperature dependences of EPR spectra' parameters were obtained for vacuum-processed samples within the range 4–600 K. Intensity vs. T plots may be well-fitted by the combination of Curie–Weiss and temperature-independent Pauli susceptibility contributions. The latter one increases on heat treatment. Significant extension of electron spin-lattice relaxation time on decreasing temperature was found.

1. Introduction

Nanocarbons with an extended π-electron system (activated carbon fibers, nanotubes, nanographite) have been a subject of special interest for the last decade. Unlike fullerenes, the π-electron network in these systems is not closed and has open edges which are directly responsible for some unconventional electronic and magnetic properties [1]. According to the theoretical predictions [2] nonbonding π-electron states with a sharp density-of-states (DOS) peak arise in the close vicinity of the Fermi level (E_F) in a flat nanographene sheet with the zigzag-type edge. These states give rise to localized spins responsible for unconventional Curie paramagnetism found in these materials [3]. Nanographite particles with the mean size 5–6 nm are characterized by the highest value of edge-localized spin concentration. Nevertheless, interaction between the edge-localized spins and the itinerant π-carriers propagating along the interior regions of graphene sheets is still not well understood. In this research we combine the methods of magnetic susceptibility and Electron Paramagnetic Resonance (EPR) aiming to distinguish between the conductive spin carriers and the edge-localized spins (having their wave-function extended along the periphery of graphene sheets) in polycrystalline samples of multi-shell nanographites. The latter were obtained by high temperature (HT) heat treatment of detonation ultrananocrystalline diamonds.

2. Experimental

Monodispersed nanographite particles were produced by annealing of detonation nanodiamonds (grain size ~5 nm) in argon atmosphere at 1600°C, as described in [4]. About 80–100 mg of the acid-treated nanodiamond powder (well purified from transition metal impurities) was loaded in a graphite crucible and heated in an electrical furnace under argon flow (1.5–2.0 l/min) at a pressure of 1.47 bar. The exposure time was taken to be 7 min and ~2 h at the peak temperature. The heating time from the room temperature (RT, T~300 K) to the maximum temperature of 1600 °C was about 35 min. The crucible temperature was controlled by an optical pyrometer through the quartz windows in the furnace. Samples from each of two series (A and B, differing by the origin of starting nanodiamond product) were exposed to the same annealing intervals: 7 min and

* Corresponding author. Ioffe Physico-Technical Institute, Polytechnicheskaya 26, St. Petersburg, 194021, Russia. Tel.: +7 812 9045298; fax: +7 812 2970073.
E-mail address: osipov@mail.ioffe.ru (V.Y. Osipov).

0925-9635/$ – see front matter © 2008 Elsevier B.V. All rights reserved.
doi:10.1016/j.diamond.2008.09.015

~2 h. We marked these samples as A7, A110, B7 and B120 (here the number means the exposure time in minutes at the peak temperature of 1600 °C).

Structure of the particles was studied by high-resolution transmission electron microscopy (HRTEM) and X-ray diffraction (XRD). The HRTEM images were taken with a JEOL JEM2010 FEF instrument (acceleration voltage 200 kV) and the XRD profiles were obtained using a Rigaku RINT2400 instrument (Cu target, 50 kV, 120 mA).

Magnetic susceptibility and magnetization measurements were carried out with a Superconductor Quantum Interference Device (SQUID) magnetometer (Quantum Design Co., MPMS-5) in the temperature range of 1.9–380 K in magnetic fields up to 5.5 T. The registration of temperature dependence of the magnetic susceptibility was carried out in a constant magnetic field, $H=0.7$ T, upon slow heating. Samples for the SQUID measurements (A- and B-series; ~20–25 mg) were packed into a capsules made from a thin aluminum foil and thereafter vacuum-sealed in quartz tubes after the treatment at 400 °C for 3.5–4.5 h at the vacuum levels better than 2.7×10^{-6} bar.

Temperature EPR measurements ($4\ \mathrm{K}\le T\le 600$ K) were carried out using a Bruker EMX-220 X-band ($\nu\sim9.4$ GHz) spectrometer equipped with an Oxford Instrument ESR900 cryostat. For temperature measurements the samples (3–7 mg) were vacuum-sealed in capillary tubes at the vacuum levels better than 3×10^{-6} bar at RT (A-series) and after the heat treatment at 300 °C for 6–7 h (B-series). Temperature dependences of resonance field H_r, peak-to-peak linewidth ΔH_{pp} and doubly integrated intensity (DIN, proportional to the EPR susceptibility χ_{EPR}) were analyzed. Electron spin-lattice relaxation times T_{1e} were estimated using progressive microwave power saturation technique.

3. Results and comparative analysis

XRD data reveal all nanographite particles under study have the same crystalline structure and the same sizes of coherent scattering region in directions along and perpendicular to the (002) graphene planes. HRTEM observations convincingly evidence that annealing at 1600 °C leads to the almost complete transformation of the nanodiamond particles to quasi-spherical carbon onions after the first few minutes of the process (see insets in Fig. 1(a)). Some onion-like particles consist of 7–8 defective spherical shells enclosed into one another with an average intershell spacing of 0.34–0.35 nm. Further graphitization converted quasi-spherical onions to polyhedral nanographite particles with an empty core as the annealing time was increased to 2 h. Some well graphitized polyhedral particles have nearly flat facets and consist of 6–8 polyhedral graphitic shells enclosed into one another with an average interlayer spacing of 0.34–0.35 nm. The mean interlayer spacing of 0.345 nm between the graphitic shells found experimentally from HRTEM images and X-ray diffraction data is a little bit greater than the 0.335 nm spacing for bulk graphite. Therefore, it means the lack of three-dimensional ordering and the "turbostratic" character of both quasi-spherical and polyhedral nanographite particles.

In nanographites the experimentally observed magnetic susceptibility (χ) may be expressed as the sum of the four terms: $\chi=\chi_{CW}+(1/3\times\chi_{orb})+\chi_{core}+\chi_{Pauli}$. Here $\chi_{CW}=C_1/(T-\Theta_1)$ is the Curie–Weiss term (where C_1 and Θ_1 are the Curie constant and Weiss temperature, respectively) and χ_{orb}, χ_{core} and χ_{Pauli} are the in-plane orbital susceptibility in the magnetic field normal to the graphene planes, the core diamagnetic susceptibility of carbon atoms and the Pauli susceptibility of conductive carriers, respectively [4]. The last three terms are either independent of temperature (χ_{core}, χ_{Pauli}) or very weakly depend on it (χ_{orb}). In order to analyze the χ_{CW} term let us suppose that $(1/3\times\chi_{orb})+\chi_{core}+\chi_{Pauli}\approx\chi_0=\mathrm{const}$ (χ_{core} is about -0.4×10^{-6} emu/g). This assumption works quite well at $T<100$ K, where the χ_{orb} is practically temperature-independent. Thus, we can experimentally investigate the spin paramagnetism in nanographites by analyzing $(\chi-\chi_0)$ vs. T below 100 K, where χ_o is a temperature-independent term in the experimentally measured magnetic susceptibility. Fig. 1(a) shows dependences of the inverse susceptibility $(\chi-\chi_0)^{-1}$ vs. T for samples A7 and A110. For getting these plots the unique χ_0 values were found by the fit procedure that leads to linear dependences in the Curie–Weiss coordinates. Indeed, it is clearly seen from Fig. 1(a) that $(\chi-\chi_0)$ satisfies quite well the Curie–Weiss law at $T<80$ K. The concentrations of localized spins (N_s) are determined as 6.1×10^{18} spins/g (A7) and 3.6×10^{18} spins/g (A110). These are exactly the same spins which are localized at the zigzag edges of nanographene sheets along its perimeters and also responsible for the appearance of a broad DOS peak around the Fermi level as well as broad EPR lines originating from nonbonding π-electrons. Thus, the concentration of localized spin drops from 6.1×10^{18} to 3.6×10^{18} spins/g when the HT treatment interval increases from 7 to 110 min. Following the spin density recalculations reported in [4], we can say the prolongation of HT treatment leads to the decrease of spin concentration from 1.4 to 0.8 spins per nanographite particle with the mean diameter 6 nm.

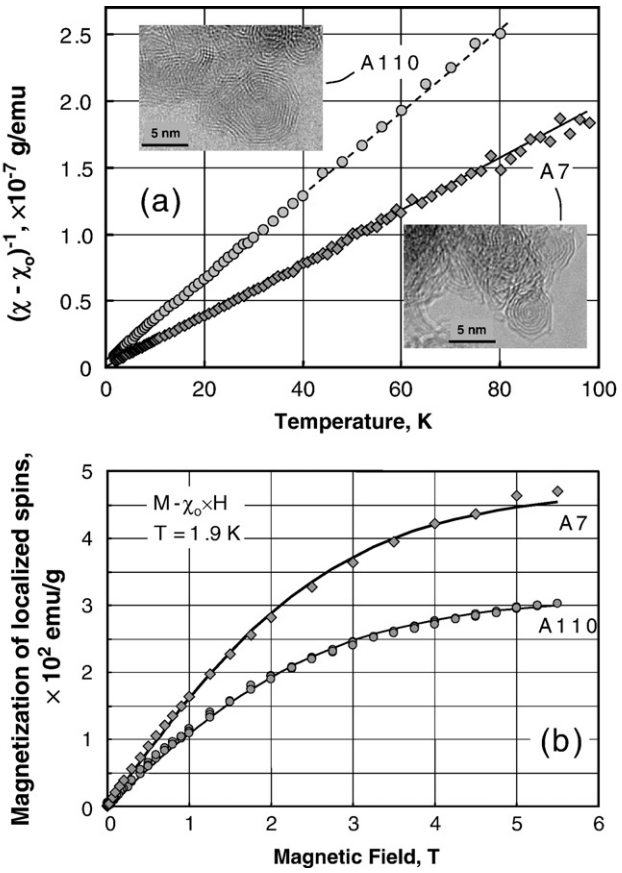

Fig. 1. (a) The dependence of inverse susceptibility $(\chi-\chi_0)^{-1}$ versus temperature (T) for the samples A7 and A110 (so-called Curie–Weiss plots). These plots are fitted well by straight lines at $T<80$ K. In the inserts: the HRTEM images of the correspondent samples. (b) The magnetization of localized spins ($S=1/2$) versus magnetic field registered at lowest temperature ($T=1.9$ K) for the A7 and A110 samples. These plots are fitted well by a Brillouin curve with $S=1/2$ and yield a concentrations of localized magnetic moments in A7 and A110 as a fitting parameters.

Subsequent study of the magnetic properties on these samples, done using SQUID magnetometer at lowest available temperature $T=1.9$ K, shows that the spin paramagnetism in all nanographites under study may be associated solely with the localized spins $S=1/2$ ($g=2.00$). It originates from the magnetization ($M-H$) curves measured at $T=1.9$ K in magnetic fields H up to 5.5 T, which may be interpreted as being a sum of the temperature-independent linear ($M-H$) segment with a negative slope $\chi_0\times H$ (here found fitting parameters $\chi_0=-1.73\times10^{-6}$ emu/g and $\chi_0=-1.99\times10^{-6}$ emu/g for the samples A7 and A110, respectively), and the characteristic curve with a positive contribution of $S=1/2$ which has

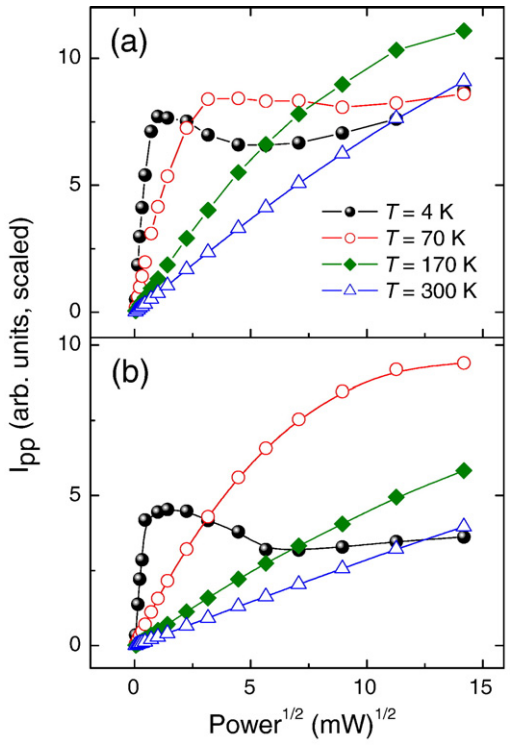

Fig. 2. Temperature dependences of microwave power saturation curves for nanographite samples B7 (a) and B120 (b).

a saturating trend in high magnetic field. The latter contribution, i.e. the difference $M-\chi_0\times H$, being well-fitted to the so-called Brillouin curve with $S=1/2$ and $g=2.00$ (Fig. 1(b)) yields an effective (i.e. observed in this experiment) concentration of localized magnetic moments of 5.4×10^{18} spins/g (A7) and 3.5×10^{18} spins/g (A110). These data for the concentration of localized magnetic moments (N_M) coincide well with the data for concentration of localized spins obtained from the Curie constants (C_1). Nevertheless, for the sample A7 (with a higher N_s value) the N_M is a little bit smaller than N_s due to short-range antiferromagnetic interaction between the neighboring edge-localized spins of the same isolated nanoparticle at $T=1.9$ K.

RT EPR spectrum of short HT treated sample A7 recorded at ambient conditions, show superposition of slightly asymmetric broad ($\Delta H_{pp}=15\pm1$ mT) line with $g=2.0015(5)$ and weak narrow ($\Delta H_{pp}\sim0.5$ mT) one with $g=2.0022(1)$. Sample B7 shows singlet Lorentzian-like line with ($\Delta H_{pp}=4.4\pm0.5$ mT). Long HT treated samples A110 and B120 demonstrate narrower intensive Lorentzian-like signals with linewidths 3.1 and 2.8 mT, respectively. The latter signals demonstrate similar (within the experimental error) g-values of 2.0012–2.0014. Concentrations of EPR active spins in the parallel pairs of samples from two series are found to be close ones (within the experimental error of 0.2×10^{19}) and estimated as 1.0×10^{19} spins/g and 1.8×10^{19} spins/g for the short and long HT treated samples, correspondingly. In full agreement with [4] EPR signals in all samples demonstrate high sensitivity to ambient dioxygen: their linewidths reduce and the peak intensities enhance on vacuum-processing. Progressive saturation measurements on vacuum-sealed samples reveal remarkable extension of electron spin-lattice relaxation times T_{1e} on decreasing temperature. Fig. 2 shows saturation curves for samples B7 and B120 obtained at various temperatures. Each point in Fig. 2 was collected with at least 10 min delay to ensure samples' temperature stabilization. Avoiding saturation effects, all temperature dependences of the EPR line parameters were recorded at microwave power levels of 50–200 μW with the temperature stabilization at each point. Fig. 3(a) demonstrates temperature dependences of $\chi_{EPR}\sim$DIN for all samples under study. It is clearly seen that samples of A-series expose abrupt drop of integral intensities at temperatures $T_p=65$ K (A7, black circles) and $T_p=12.5$ K (A110, open circles). Samples from B-series also demonstrate some peculiarities (slowing down or even leveling of the intensities' growth) at $T<20$ K. Within the temperature regions between $T_p\le T\le600$ K (A-series) and 20 K$\le T\le$600 K (B-series) the high frequency ac-spin susceptibilities of EPR active species χ_{EPR} may be well described by the following equation $\chi_{EPR}=\chi_{Pauli}+C_2/(T-\Theta_2)$ which combines the

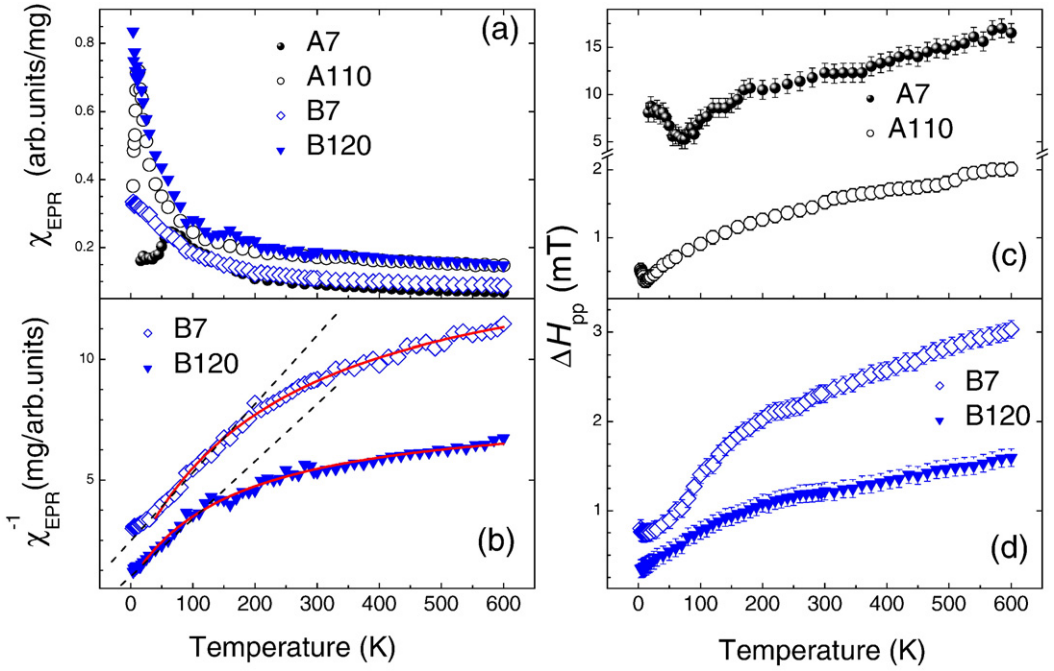

Fig. 3. Temperature dependences of: (a) EPR susceptibility $\chi_{EPR}\sim$ DIN for nanographite samples of series A and B; (b) inverse EPR susceptibility $(\chi_{EPR})^{-1}$ for nanographite samples of series B. Black dashed lines represent the Curie–Weiss dependence. Red solid lines represent best linear fit by $\chi_{EPR}=\chi_{Pauli}+C_2/(T-\Theta_2)$; EPR linewidth ΔH_{pp} for nanographite samples of series A (c) and B (d).

Curie–Weiss and the temperature-independent Pauli paramagnetic contributions. Here C_2 and Θ_2 are the effective Curie constant and Weiss temperature allowed for all EPR-visible groups of spins presented in the system. Fig. 3(b) shows best linear fits of inverse EPR susceptibility using the combined Curie–Weiss–Pauli equation (red solid lines) in comparison with the Curie–Weiss behavior (black dashed lines). It is clear that at $T>70$–100 K just the Pauli contribution due to conducting carriers dictates behavior of EPR lines intensities. The following values for χ_{Pauli} are determined by fitting (in arb. units/mg): A7—0.05 (±0.01), A110—0.13 (±0.01), B7—0.07 (±0.01) and B120—0.12 (±0.01). It evidences that prolongation of HT treatment results in strengthening of the Pauli susceptibility contribution. Fig. 3(c) and (d) demonstrate temperature behavior of linewidths. In parallel with the intensities, at low temperatures ΔH_{pp}'s pass through minima at T_{p} (A-series) and slowing/leveling region (B-series). Above these specific regions the ΔH_{pp}-values gradually increase for all samples under study.

Our EPR measurements evidence that in nanographite samples under study the concentrations of all EPR active spins exceeds the concentrations of the edge-localized spins obtained by magnetic susceptibility measurements. The discrepancies in concentrations are 1.6–5.0 times in favor of EPR obtained concentrations. The most remarkable it sounds for the long HT treated samples. Such a difference may originate in the presence of conductive π-carriers propagating in the interiors of graphene sheets that are responsible for the appearance of the temperature-independent Pauli susceptibility in these systems. The concentrations obtained from the Curie–Weiss plots described above obviously cannot include the carriers' contribution correctly, especially for the samples undergone longer HT treatment where the Pauli contribution is found to be significantly large. Type and amount of conductive carries (π-electrons or hole carriers) in each individual particle of the whole ensemble of nanographite particles [5] depend upon the position of Fermi level relative to the contact point where π- and π*-bands touch each other. E_{F} can locates in the valence π-band or conductive π*-band, but its absolute mean value is not too large (≤0.11–0.12 eV). In this case the total amount of degenerate conductive carries in a single nanographite particle (size 6 nm) does not exceed 6–7.

Susceptibility measurements show in short HT treated samples the average number of edge-localized spins per particle exceeding 1 that, probably, leads to antiferromagnetic exchange interaction between the spins belonging to the same particle. This exchange interaction may cause the low temperature peculiarities in both DIN and linewidth (see Fig. 3) found in samples of two series. The difference in low temperature behavior of EPR parameters between the series may arise due to subtle differences in structure of starting materials and\or amount of adsorbed gases (the further study is in progress). The same interaction as well as interactions between edge-localized and conductive carriers' spins supposed to be responsible for the broadening of EPR lines in vacuum-sealed samples. The actual linewidth is determined by the competition of three processes: 1) magnetic interaction between the edge-localized spins; 2) nonbonding π-electron scattering on the edge-phonon modes localized on the periphery of the graphene sheets; and 3) spin-lattice relaxation. Slowing down of the spin-lattice relaxation rate is responsible for the reduction of EPR linewidth with temperature decrease down to T_{p}. Competition between these processes leads to the complicated linewidths behavior observed. Thus, at $T<T_{\mathrm{p}}$ one can observe line broadening/leveling together with the substantial extension of electron spin-lattice relaxation time. This collision may be understood in terms of attenuation of interactions between edge-localized and carriers' spins (possibly due to localization of the conductive carriers) and strengthening of antiferromagnetic fluctuations.

In conclusion, both magnetic susceptibility measurements and EPR show that high temperature annealing of detonation nanodiamond leads to radical transformation of dielectric and paramagnetic (predominantly sp^3) nanodiamond particles into sp^2 nanographitic π-electronic systems with complex electronic and magnetic characteristics which properties strongly depend on heat treatment and samples' preparation conditions. The concentrations of all EPR active spins in nanographites exceed the concentrations of the edge-localized spins estimated by magnetic susceptibility measurements. This difference originates in the presence of conductive π-carriers propagating in the interiors of graphene sheets which number depend upon the position of Fermi level. Just these spins mediate magnetic interaction between distant spins localized on the opposite zigzag edges/sides of the nanographite particle.

Acknowledgements

V. Yu. O. thanks the Japanese Society for the Promotion of Science (JSPS) and the Tokyo Institute of Technology for the fellowship and financial support in FY 2004/2005, 2008. Authors also thank New Energy Development Organization of Japan (NEDO, grant #04IT4) for the financial support. A. Ya. V. and V. Yu. O. thank the Russian Federal Agency for Science and Innovation for the financial support in the frame of project 2007-3-2.3-07-02-00.

References

[1] M. Fujita, K. Wakabayashi, K. Nakada, K. Kusakabe, J. Phys. Soc. Jpn. 65 (1996) 1920.
[2] K. Nakada, M. Fujita, G. Dresselhaus, M.S. Dresselhaus, Phys. Rev., B 54 (1996) 17954.
[3] Y. Shibayama, H. Sato, T. Enoki, M. Endo, Phys. Rev. Lett. 84 (2000) 1744.
[4] V.Yu. Osipov, T. Enoki, K. Takai, K. Takahara, M. Endo, T. Hayashi, Y. Hishiyama, Y. Kaburagi, A.Ya. Vul', Carbon 44 (2006) 1225.
[5] K. Takai, M. Oga, H. Sato, T. Enoki, Y. Ohki, A. Taomoto, K. Suenaga, S. Iijima, Phys. Rev., B 67 (2003) 214402.